Proceedings of the Institution of Mechanical Engineers, Part D: Journal of Automobile Engineering, Volume 230, Issue 6, pp. 841-854
DOI: 10.1177/0954407015596274

Aerodynamic characteristics of a wing & flap configuration in ground effect & yaw

Luke S Roberts[1], Joao Correia[2], Mark V Finnis[1] and Kevin Knowles[1]

Abstract

The influence of yaw on a model representative of a monoposto racing car front wing and nose section operating in close proximity to the ground is discussed. The yawed condition is representative of a car operating in a cross-wind or with side-slip whilst cornering. Due to the need for downforce in corners rather than on a straight it is standard practice to test a racing car at varying orientations of yaw, pitch and roll quasi-statically. Wind tunnel testing with a 50% scale model at a chord-based Reynolds number of 1.69 x 10^6 /m was used to investigate forces and surface flow structures. The results were then used to validate simulations with the 3-equation k-k_L-ω transitional turbulence model to observe surface pressures and wake structures. It was found that a change of surface pressures caused asymmetric loading of the wing, the strengthening or inhibiting of vortices depending on their rotational sense, and an overall reduction in both the downforce and drag of the wing; all of which were amplified as yaw angle was increased or ground clearance reduced. The fundamental aerodynamic flow features of a racing car front wing operating at yaw are established.

Keywords

Wind tunnel, CFD, transitional model, race car, crosswind, side slip, cornering

Nomenclature

A	Wing planform area /m^2
c	Total wing & flaps chord /m
C_L	Lift coefficient $\left(\frac{L}{q_\infty A}\right)$
C_D	Drag coefficient $\left(\frac{D}{q_\infty A}\right)$
C_F	Skin friction coefficient $\left(\frac{\tau}{q_\infty}\right)$

[1] Aeromechanical Systems Group, Cranfield University, UK
[2] Amlin Aguri Formula E Team, UK

Corresponding author:
Luke Roberts, Aeromechanical Systems Group, Cranfield University, Defence Academy of the United Kingdom, Shrivenham, SN6 8LA, UK.
Email: l.roberts@cranfield.ac.uk

C_P	Pressure coefficient $\left(\frac{\Delta P}{q_\infty}\right)$
D	Drag force /N
h	Ground clearance /m
L	Lift Force (positive upwards) /N
ΔP	Local static pressure relative to freestream /Nm^{-2}
q_∞	Freestream dynamic pressure /Nm^{-2}
Q	Positive second invariant of Jacobian /s^{-2}
S	Strain rate /s^{-1}
U_∞	Freestream velocity /ms^{-1}
U_*	Shear velocity $\left(\sqrt{\frac{\tau}{\rho}}\right)$ /ms^{-1}
x_{sep}	Chordwise separation point
$x_{reattach}$	Chordwise reattachment point
x, y, z	Cartesian coordinates (x – downstream, y – vertically down, z - horizontal)
X	Total model length /m
Y^+	Dimensionless wall distance $\left(\frac{U_* Y}{\nu}\right)$
Y	Distance to nearest wall /m
Re	Chord-based Reynolds number $(\frac{U_\infty c}{\nu})$
ν	Kinematic viscosity /m^{2}s^{-1}
τ	Local wall shear stress /Nm^{-2}
Ω	Vorticity magnitude /s^{-1}
$\bar{\Omega}$	Normalised vorticity magnitude (by maximum value across all measurement planes)

1. Introduction

The study of inverted wings operating in close proximity to a ground plane has been the subject of much research in the past decade [1-11]. All the published information, however, relates to a wing orientated with its axis of symmetry parallel to the freestream wind direction. In practice a wing must operate over a wide range of operating conditions. Whilst the effect of altering ground clearance and pitch are important and have been extensively studied, the yaw condition has been seemingly forgotten. Yawing of the front wing of a racing car simulates the cornering condition, which is when maximum grip, and hence downforce, is primarily required.

The aim of a racing car is to navigate a track in the minimum time possible; in order to do this it requires a consistent and stable aerodynamic platform. As a racing car must operate over a wide range of car speeds and attitudes throughout a lap it is important to understand the aerodynamic characteristics of the car not only in a straight line. Quasi-static testing of the car over a range of orientations is usually performed to understand how the performance of the car alters during the cornering manoeuvre, which consists of pitching, heaving, yawing and rolling motions, to ensure consistent downforce production and understand attitude changes due to centre of pressure movements during the manoeuvre. The importance of aerodynamic balance and a comprehensive overview of race car aerodynamics can be found in Dominy [11] and Zhang et al. [12].

The dynamics of a race car during a cornering manoevre are shown in Figure 1. As the race car navigates a corner two yaw effects are generated, constant yaw angle (°) due to side slip, and the dynamic yaw rate, or rate of change of yaw angle (°/sec), as the vehicle rotates about its centre of gravity. Therefore, the front and rear of the car will experience different yaw angles as the car rotates about its centre of gravity while moving in an arc of assumed constant radius. Thus, in the rotating reference frame the airflow has centripetal acceleration and Coriolis-effect terms. These terms make simulating the true cornering condition almost impossible to recreate in a standard automotive wind tunnel as it introduces a velocity gradient with constant static pressure. Simply building a wind tunnel with a curved test section would not satisfy these conditions as static pressure would not remain constant.

The yaw rate for a racing car can be high, up to 50 °/sec, but is only significant aerodynamically during quick change of direction events, such as initial turn-in to the corner. The yaw angle, however, is felt throughout the corner and is usually in the vicinity of 3-5°. Although the yaw angle changes throughout the corner the yaw rate is not sufficiently high, other than for the initial turn-in event, to warrant any more than quasi-static analysis; as was shown to be true by Molina & Zhang [13] for a heaving wing. So whilst racing car designers do evaluate true cornering in computational fluid dynamics (CFD) through the use of a curved domain with additional terms applied [14], it is usually to help understand the difference between the track and wind-tunnel rather than actual aerodynamic development.

It is for these reasons, as well as the fact that the difference in flow angle between the leading and trailing edges of the wing in curved flow are minimal (and insignificant compared to those on a full car), that only the quasi-static testing of yaw is observed in this study.

The front wing generates approximately 30% of a Formula One car's total downforce [15], however, the design is also dictated by the flow structures it produces, which will interact with downstream features. As the first

component to interact with the airflow, the front wing must condition the flow to ensure downstream components operate in high-energy flow with low turbulence intensities. Hence, the front wing can have a dramatic effect on the performance of components such as the underbody and rear wing.

In this work a wing has been studied in isolation, however, it should be noted that in real-world conditions the car will be subjected to varying yaw angles not just from side slip and crosswind, but also from interactions with other cars [16-20].

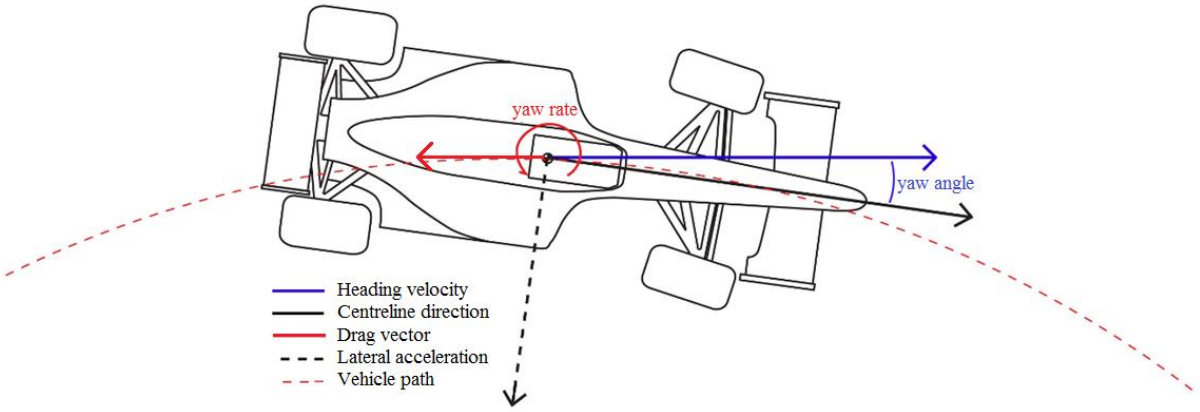

Figure 1. Diagram showing a race car attitude in cornering

The present study aims to further the understanding of inverted wings in ground effect operating at yaw by analysing how their aerodynamic characteristics change, both on and off the surface. A simplified model of the front-wing assembly of a monoposto racing car has been used for this study; although there is potential for strong flows originating from other downstream features, this approach allows the effects due to the wing alone to be observed.

2. Related work

A wing operating in close proximity to the ground has been shown to be dependent on ground clearance [3-10]. As the wing moves closer to the ground its downforce increases, primarily due to the constraining of flow between the wing and ground; a secondary force-enhancement mechanism is the tip vortex, which forms due to the pressure gradient between the upper and lower wing surfaces, with the endplate geometry also having an effect on its formation. Zhang and Zerihan [9] showed that a wing-tip vortex enhances downforce due to the region of high suction it generates at the tip. At lower ground clearances this vortex bursts, negating its force-enhancement mechanism, but the constraining of flow between the wing and ground still causes downforce to increase. At even lower ground clearances a critical point is reached where the boundary layer separates and the wing enters the so-called force-reduction region (as seen in Figure 4a, discussed later).

A wing operating out of ground effect, with varying endplate configurations, and set at 0° and 20° yaw was computationally analysed by Gogel & Sakurai [21]. While such a high yaw angle is not representative of the angles which would be experienced by a monoposto racing car when running normally on a track, the results are still a good indication of what can be expected when operating a wing with endplates at yaw. The authors found that applying yaw to the model caused downforce to reduce by up to 9.63% (depending on endplate configuration) due to separation from the windward endplate reducing the mass flow over the wing's suction surface. On the leeward endplate pressure was increased on both the pressure and suction surfaces due to the stagnation of air on the inside of the endplate. This contributed to the net decrease in downforce.

3. Description of study

3.1 Test facility

Experiments were conducted in Cranfield University's DS Houghton wind tunnel, a 2.7 m x 1.7 m closed-return, three-quarter-open test section wind tunnel, at the Defence Academy of the UK, Shrivenham. The facility is equipped with a continuous-belt rolling road, which is synchronized with the freestream velocity, and boundary-layer suction applied through perforated plates ahead of the road. The optimisation and distribution of this suction combined with a knife-edge transition to the belt gives, in test conditions, a boundary layer thickness of 1.58 mm and freestream turbulence of 0.3% at the leading edge of the model at a freestream velocity of 25 ms^{-1}. It uses Pi Research Ltd's "Mistral" wind tunnel control and acquisition system, which was originally designed for Formula One wind tunnel applications. This system controls all aspects of the wind tunnel's operation and acquisition of data from all sensors. An overhead sting with an automated motion system both supports the wing and accurately adjusts the model's ground clearance during the experiment through "templates" created in the Mistral software. Further information on this tunnel is given by Knowles & Finnis [22].

3.2 Test Model

Tests were conducted on a simplified monoposto racing car front wing (Figure 2). This consists of an untapered, untwisted, rectangular-planform, GAW-(1) section main-plane of span 750 mm and chord 119.7 mm set at -0.5° incidence, with two Reynard Racing "Kylie" flaps of 250 mm span and 160 mm chord orientated at 23.9° incidence and with rectangular endplates. The wing was suspended by two vertical pylons, similar to the front wing pylons of a racing car, from a six-component Aerotech force balance housed inside a non-metric (i.e. not connected to the force balance) streamlined body of 600 mm length. Thus, although the body had an aerodynamic

influence on the wing, in which respect it mimicked the nose section of a car, the forces generated on the body itself were not measured.

It is clear that the model is an extremely simplified variant of that seen on a modern Formula One car, which uses highly complex three-dimensional endplates that are designed predominately to manage yaw effects and interaction with the front wheels. Although the rectangular endplates used in this study are not as complex as those used in Formula One, the fundamental aerodynamic characteristics which they possess are representative and are adequate to give an understanding of the flow field. Furthermore, outside of Formula One there are numerous monoposto racing series which utilise 'two-dimensional' design endplates similar to these.

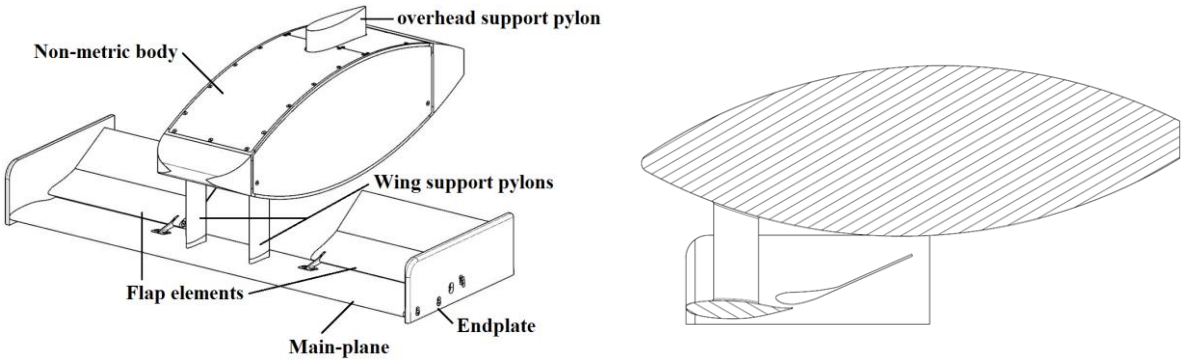

a) b)

Figure 2. *(*a) Schematic of front wing model and *(*b) centre-line section view

3.3 Experimental Method and Uncertainties

Force measurements were taken at yaw angles of 0°, 2.5° and 5° at a range of non-dimensional ground clearances of h/c = 0.89 to h/c = 0.06. The yaw angle was defined as the angle between the centrelines of the wing and wind tunnel test section. Although yaw angles can exceed this on the track, up to only 5° was tested as this was the maximum to which the model could be set on the support strut. Experiments were conducted at a Reynolds number of 4.75 x 10^5, based on the total chord length (main-plane and flap) and freestream Mach number of 0.0776, based on the freestream wind temperature and velocity.

The ground clearance was defined as the distance from the lowest point of the wing's suction surface to the road. The model was positioned to an accuracy of ±0.0019° in yaw, ±0.0037° in roll, and ±0.0015° in incidence. The wind tunnel speed was regulated by the Pi Mistral control system, based on ambient temperature and pressure, to maintain a constant chord-based Reynolds number of 4.75x10^5 ±470. This is representative of typical wind tunnel test values for a 50% scale F1 model.

Before and after each run wind-off data were acquired in order to account for any offsets in the measurements during the experiment. Force data were then acquired at each ground clearance for 20 seconds at a frequency of 10 Hz. The uncertainty in recorded drag and lift coefficients was calculated to be ±0.0023 and ±0.014 respectively at a 95% confidence level. This calculation was based on all parameters which affected the experiment including model orientation, force balance error, and wind tunnel operating conditions. The uncertainty associated with each variable was calculated by doing a parametric study where each variable was changed individually and tested at two different settings. It was then assumed that the resultant variation caused by each variable was linear between the two tested settings. The uncertainty was then calculated by using these results and the uncertainty associated with the accuracy of each setting.

Flow visualisation on the suction surface of the wing was conducted using a paint based on a mixture of fluorescent pigment, oleic acid and paraffin. The paint was sprayed on the suction surface immediately prior to the running of the tunnel. The wing was run in the tunnel at a constant Reynolds number for 45 minutes in which time the flow pattern dried on the surface. The wing was then removed and taken to a dark room where photographs were taken under ultra-violet light.

3.4 Computational Method

Simulations were completed using the commercial software ANSYS Fluent 15.0.7 [23] on the full wing and nose section assembly on Cranfield University's high performance computing network, Astral. This comprises a dedicated cluster of nodes with a total of 1280 cores available and a peak measured performance of 18.8TFlops. For simulations in this study 64 CPU cores, giving 256GB of shared memory, were used.

Some simplifications were made to the model in order to make mesh generation easier and improve the spatial discretisation of the volume; these were the removal of a bracket which held the flap, rounding edges where the vertical pylons met the wing and nose, and the elimination of the overhead support strut. The bracket was removed as it compromised the quality of prism and volume elements in the already confined space between the main-plane and flap. The large number of prism elements affected this, but correct representation of the transitional boundary layer was perceived as more important aerodynamically than the influence of the bracket. The rounding of edges on the support pylons were small enough not to have a significant effect on the flow-field, but still aided in mesh generation. Although each of these modifications may have had some influence on the flow-field, since the output is comparative and all simulations will be similarly affected, the trends shown by the results are valid.

The volume was discretised into between 28 and 30 million (depending on configuration) unstructured surface and volume elements with a domain spanning 3X upstream and 7X downstream of the model using Ansys ICEM

CFD [24]. A total width of 6X and total height of 3X gave 3.7% blockage. The low blockage level and sufficient length meant that all boundaries held constant static pressure and thus were not influenced by the model. A frontal view of the mesh with boundary conditions indicated is shown in Figure 3; in this the refinement of volume elements near to the model can be seen. Of the total elements, approximately 1.2 million were triangular surface elements, 18 million prism boundary layer elements and 10 million tetrahedral volume elements with refinement completed both below the wing and in the wake region. The mesh is fine enough to eliminate grid dependency, as was concluded through a mesh-dependence study. It is believed that the refinement of volume elements above the wing could have been reduced; however, since the computation time was acceptable for the study time constraints this was not investigated further. One important result of the mesh dependence study, however, was the susceptibility of the transitional turbulence model to the Y^+. It was found that simply refining into the viscous sublayer ($Y^+ < 5$) was not enough to give representative results, instead a $Y^+ < 1$ was found to be necessary to correctly capture transitional behaviour. Hence a large number of prism elements were obligatory in order to give the small Y^+ across the entire surface whilst still giving a total prism thickness large enough the encase the boundary layer and separation bubble, and keep the prism growth rate of 20%. A target value $Y^+ = 0.8$, based on freestream velocity and the wing chord, was applied to all surface regions during pre-processing. This ensured a maximum Y^+ of 1 on the wing surfaces, which was confirmed in post-processing. Particular attention was paid to the vortex core regions when refining the mesh in order to minimise the truncation error of the discretisation causing artificial dissipation of the vortices.

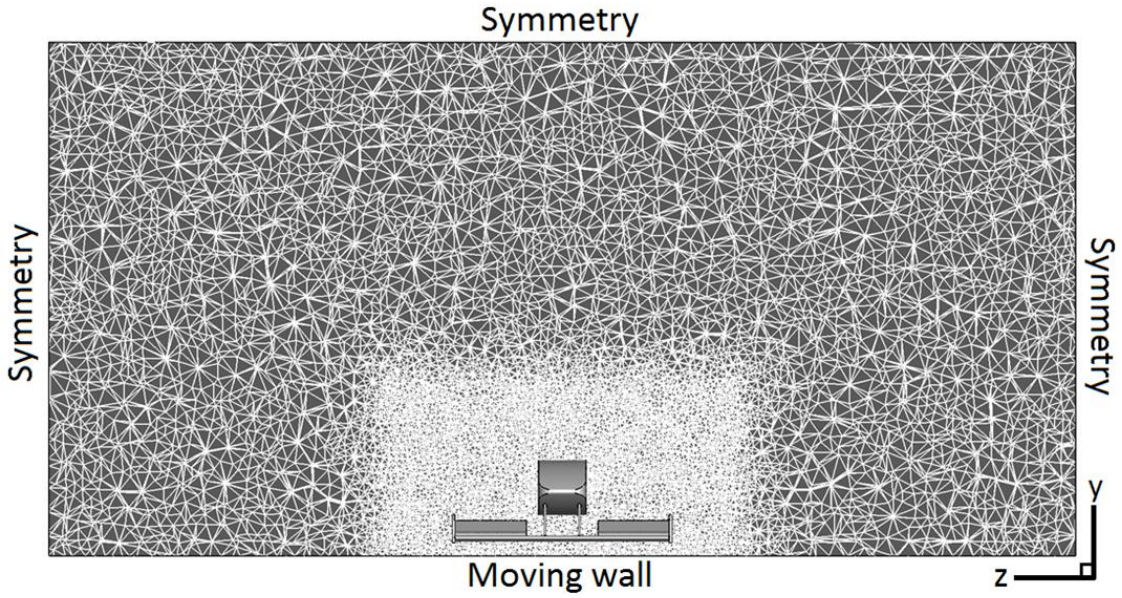

Figure 3. Frontal-view slice of volume mesh at the trailing-edge of the wing with domain boundary conditions labelled

A steady-state, incompressible, segregated solver was used with the transitional 3-equation k-k_L-ω turbulence model [25]. This model was chosen as it was capable of capturing accurately the presence of a laminar separation bubble on the wing's suction surface, which has been shown to be important in the generation of downforce for this particular wing [10]. The SIMPLE scheme was used to couple the pressure and velocity fields. Spatial discretisation of pressure was set as standard with a Green-Gauss node-based scheme for the computation of cell gradients. A second-order upwind scheme was used for the discretisation of momentum, turbulent kinetic energy (k), laminar kinetic energy (k_L) and specific dissipation rate (ω). Flow entered the domain through a velocity inlet, and exited at a pressure outlet. Symmetry boundary conditions were used for the sides of the domain as this acts as a zero-shear slip wall with zero flux across the plane. In order to replicate the movement of the wing relative to the stationary ground correctly, a moving wall set to translate in the same direction and with the same magnitude as the freestream wind velocity was used. As the freestream turbulence level reduces along the length of the domain, due to the dissipation terms, the inlet turbulence level was specified as to give freestream turbulence of 0.3% at the model.

All simulations were initialised with a zero-velocity flow-field, as recommended by Lanfrit [26], and run for 12,000 iterations, by which time the lift and drag forces had become steady state and residuals for continuity, velocity (in x, y, and z directions), k, k_L and ω all decreased below 10^{-5}. The total computation time for each simulation was approximately 35 hours (wall clock).

4. Experimental Results & Discussion

4.1 Force Measurements

Figure 4 shows the how the forces of the wing change as its yaw angle relative to the oncoming flow is increased from 0° to 5°. The change of downforce with reducing ground clearance exhibits the same behaviour found in previous studies [3-10]. As the wing moves towards the ground the downforce increases due to the constraining of flow between the wing surface and the ground. Eventually the wing reaches a critical ride height, after which downforce reduces with reducing ground clearance, known as the force-reduction region. As more yaw is imparted to the model the downforce at given ground clearances reduces in all instances. At lower ground clearances, however, there is a larger percentage of downforce lost due to the applied yaw; this culminates in a maximum downforce reduction of 3.8% for maximum yaw and minimum ground clearance.

The change in drag force is similar to that of downforce in that it reduces with yaw, particularly at lower ground clearances. In contrast to the findings of Zhang & Zerihan [8] there was a plateau and slight reduction in drag force at lower ground clearances before then increasing again at the minimum tested ground clearances. The

initial plateau could be due to the reduction of induced drag, due to the decrease in downforce, before trailing-edge separation begins to occur and pressure drag consequently increases.

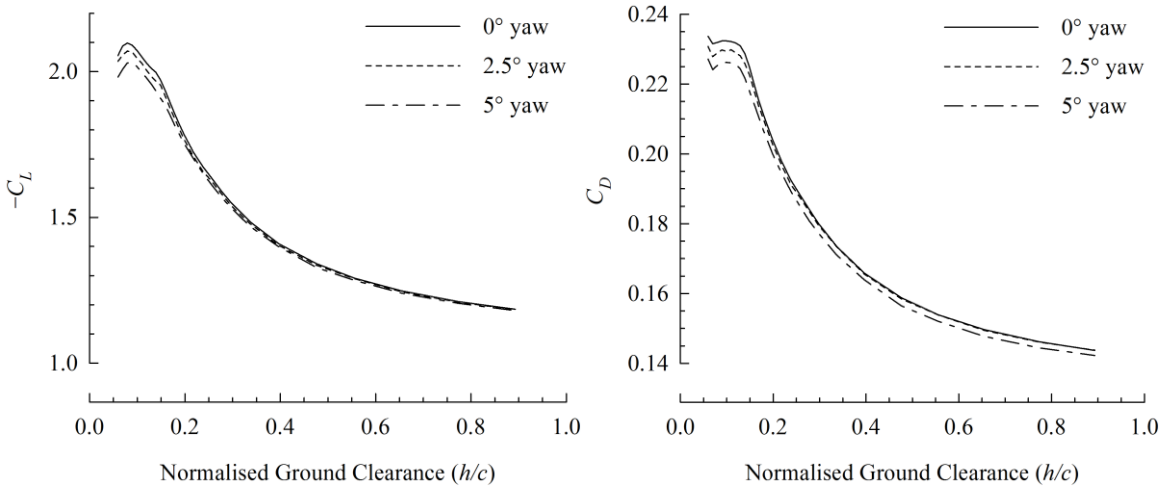

a) b)

Figure 4. Experimental a) lift and b) drag coefficients at varying yaw angle and non-dimensional ground clearance (Re = 4.75 x 10^5)

In close proximity to the ground the generation of downforce is dependent both on vortex enhancement, that is the term used to describe vortex-induced suction and laterally constrained flow, as well as the constraining of flow between the suction surface and the ground. Thus, it can be postulated that at a reference ground clearance the reduction in downforce, following yaw, must be due to the loss of vortex enhancement, as the flow is being constrained between the wing and ground equally for the straight-ahead and yawed wing.

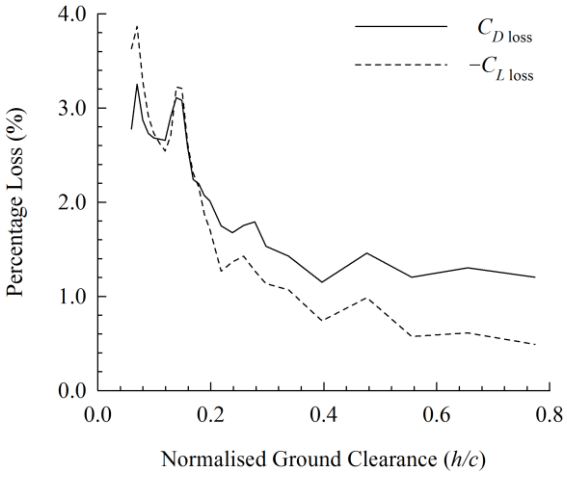

Figure 5: Percentage loss of downforce and drag due to 5° yaw compared to zero-yaw case at varying ground clearance (Re = 4.75 x 10^5)

Although the typical force vs ground clearance plots shown in Figure 4 are good for showing the overall picture of how the yawed wing forces alter with ground clearance compared to the straight-ahead wing case, they do not show the true extent of the force changes. Figure 5 shows, in terms of percentage of downforce and drag, how much force is lost. To give some perspective on the magnitude of this, Dominy & Dominy [27] showed that for a F1 car a 10% increase in downforce gave approximately one second reduction in lap time. Therefore, a 2% downforce loss on a component, which generates around 30% of the car's total downforce and which directly affects how the other two key downforce contributors function, is significant.

4.2 Flow Visualisation

Figure 6 shows photographs taken of surface flow visualisation on the suction surface of both the main plane and flap elements, as well as the inside of the endplate at 0° and 5° yaw angles. Given the small difference in downforce results, 2.14% at h/c = 0.177 and 2.88% at h/c = 0.089, it is unsurprising that only slight differences exist in the surface flow features.

The dominating feature on the main-plane suction surface is a laminar separation bubble (see Figure 6), which was previously documented for the single-element configuration of this wing and shown to be an additional force-enhancement mechanism [10]. A separation bubble on a wing forms when the laminar boundary layer separates due to the adverse pressure gradient, turbulence then grows in the separated shear layer due to inviscid Kelvin-Helmholtz type instabilities, causing reattachment as a turbulent boundary layer. Analysis of the bubble using image-processing software shows that separation occurs at x/c = 0.59 before reattaching at x/c = 0.75, giving a bubble length of 16% of the main-plane chord. However, there appears to be little or no change in the bubble's formation due to the yaw imparted upon the model, therefore the change in sectional forces must be due to either surface pressure or vortex-enhancement changes.

The wing tip vortices at either end of the main plane are visible; they originate from the leading edge of the wing where it meets the endplate and grow downstream, thus leaving a triangular-shaped pattern on the surface (red box in Figure 6a). This vortex eliminates the separation bubble close to the wing tip due to the spanwise mixing of flow. The high incidence angle of the flap means there is no evidence of the wing-tip vortex near to the endplate. The inside edge of the flap, however, shows clear signs of vortex entrainment as flow moves inward and is almost perpendicular to the freestream flow direction. This, therefore, indicates that at least four vortices originate from the suction surfaces, two from the main-plane wing tips and two from the flap's inside tips.

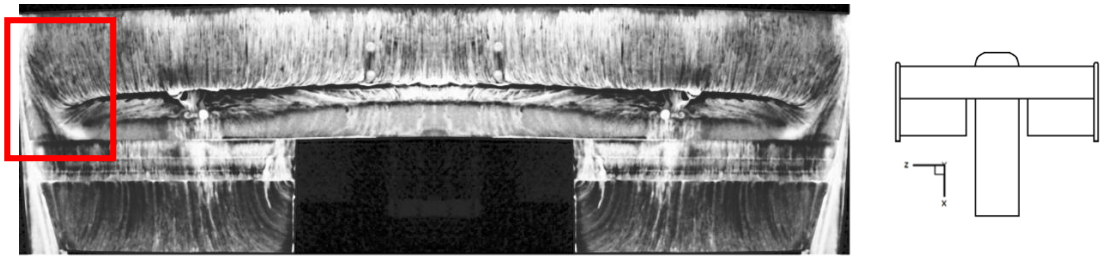

a) 0° yaw at *h/c* = 0.177

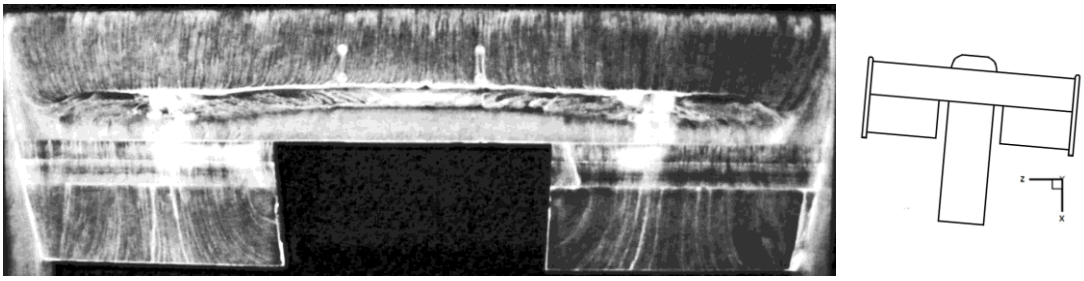

b) 5° yaw at *h/c* = 0.177

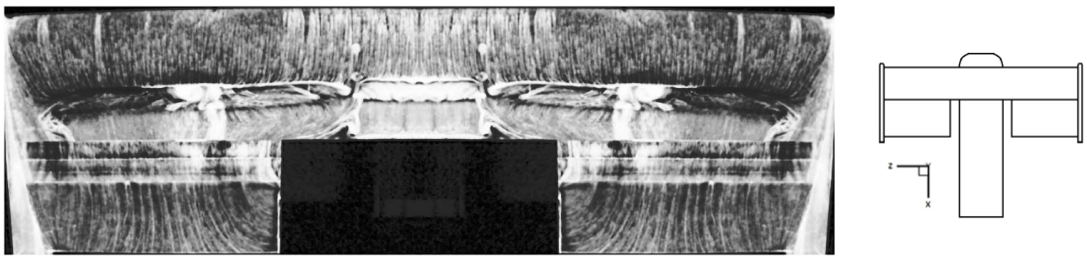

c) 0° yaw at *h/c* = 0.089

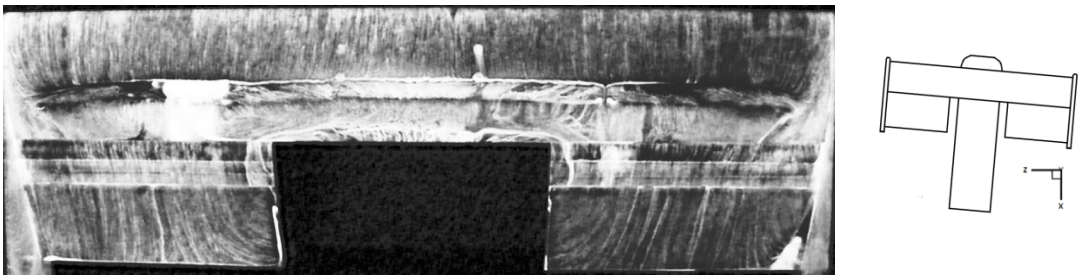

d) 5° yaw at *h/c* = 0.089

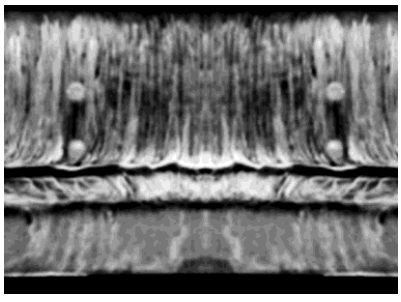

e) Schematic of surface flow regimes

Figure 6. Surface flow visualisation of suction surface at Re = 4.75 x 10^5 (flow moving top to bottom). [See text for explanation of red box in part a).]

As yaw was imparted to the model the formation of the windward tip vortex was clearly affected. The main-plane tip vortex appears larger, although the flow visualisation does not indicate whether its stability has been affected. A region of flow separation appears on the windward flap suction surface. This occurs partly due to separation, the shift in stagnation from the front of the endplate to the side, and partly because the low pressure core of the main-plane tip vortex pulls air away from that region as it moves parallel with the freestream flow.

Trailing-edge separation is observed in the central region of the wing when operating at yaw but not in the straight-ahead case. Trailing-edge separation occurs when the boundary layer no longer has enough energy to overcome the adverse pressure gradient, therefore it must be assumed that there is additional energy extraction in the yawed case. There are three possible explanations for this phenomenon, though it is most likely a combination of the three which all contribute to an overall energy loss. Firstly, as the aluminium wing surface has been milled in the streamwise direction there is increased surface roughness, due to the material grain, for air flowing spanwise across the surface. An increase in surface roughness can cause additional momentum losses in the boundary layer. Secondly, there has been a reduction in the mass-flow rate underneath the wing which reduces the energy in the flow and thus making separation more likely as it is effectively operating at a lower Reynolds number. Changes to the mass-flow rate will be investigated in the subsequent computational section. Finally, as the flow must travel further than the wing chord length due to the lateral flow component when placed at yaw. At 5° yaw there is a reduction in effective diffuser angle (taken between the lowest point of the wing and the trailing edge) of 0.03°. The effective reduction in expansion ratio of the diffuser due to the reduced angle would reduce the mass-flow rate, hence these aspects are linked. Although each of these are all small changes, when combined together it is feasible that the total energy loss is enough to cause trailing-edge separation.

5. Computational Results & Discussion

Simulations of the wing at yaw angles of 0°, 2.5° and 5° at a ground clearance h/c = 0.177 were completed in order to understand how the surface pressures and wake structures of the wing altered when operating at yaw. This ground clearance was chosen as it represents the force-enhancement regions in which tip vortices are expected still to be stable; thus allowing observations of changes in their trajectory to be made easily.

5.1 Validation

Before comments on the flow structures are made, it is important to compare the results of CFD simulations and wind tunnel testing to validate the computational method. Table 1 shows the error in the prediction of forces by CFD simulations compared to wind tunnel results to be less than 3.5% in all instances. Although simulations over-

predict drag and under-predict downforce the fact that the error is relatively consistent for each case, with a range between the largest and smallest error of 0.18 percentage points in drag and 0.35 percentage points in downforce, highlights that the overall trends shown by the CFD results are consistent with those occurring in the wind tunnel.

Table 1. Force coefficients from wind tunnel testing (WTT) and CFD simulations at *h/c* = 0.177 and Re = 4.75 x 10^5

	C_D at 0°	C_D at 2.5°	C_D at 5°
WTT	0.211	0.205	0.205
CFD	0.217	0.211	0.211
Error	2.84%	3.02%	3.01%

	-CL at 0°	-CL at 2.5°	-CL at 5°
WTT	1.826	1.807	1.795
CFD	1.764	1.745	1.739
Error	-3.40%	-3.46%	-3.11%

Figure 7, which compares surface streaklines from CFD, generated by surface shear stress vector, compared to the wind tunnel flow visualisation. The transitional turbulence model is capable of capturing the laminar separation bubble on the main plane. The region prior to initial separation and the way in which the lines become horizontal as the bubble starts show excellent correlation to the experiments, as does the region next to the endplate where the tip vortex impinges on the bubble. The main deficiencies are that the length of the bubble is too large, especially in the central region, and that there is a second flow separation after the supposed turbulent reattachment at the bubble, again in the central region. The separation is only observed in the central region due to the lack of flaps, which provide off-the-surface pressure recovery (and wakes are more resilient than boundary layers). It appears that the turbulence model does not generate sufficient turbulent kinetic energy so reattachment after the separation bubble is not turbulent but laminar; this laminar boundary layer then separates again. Turner [28] suggests that the shear sheltering term, which is included to inhibit non-linear turbulence breakdown in the pre-transitional boundary layer, is inappropriate for separation-induced transition.

On the flap, the streakline directions are identical, other than the occurrence of a separation bubble, to the flow visualisation. It is not clear whether the flap boundary layer is laminar or turbulent in wind tunnel tests, but it can

be assumed that as insufficient turbulence is produced on the main plane the bypass transition function may not have occurred for the flap, hence a bubble is seen rather than a fully turbulent boundary layer across the whole flap.

Overall, the accurate prediction of aerodynamic forces and representation of the surface flow structures gives validation to the computational method and thus the results presented in the subsequent sections can be deemed reliable.

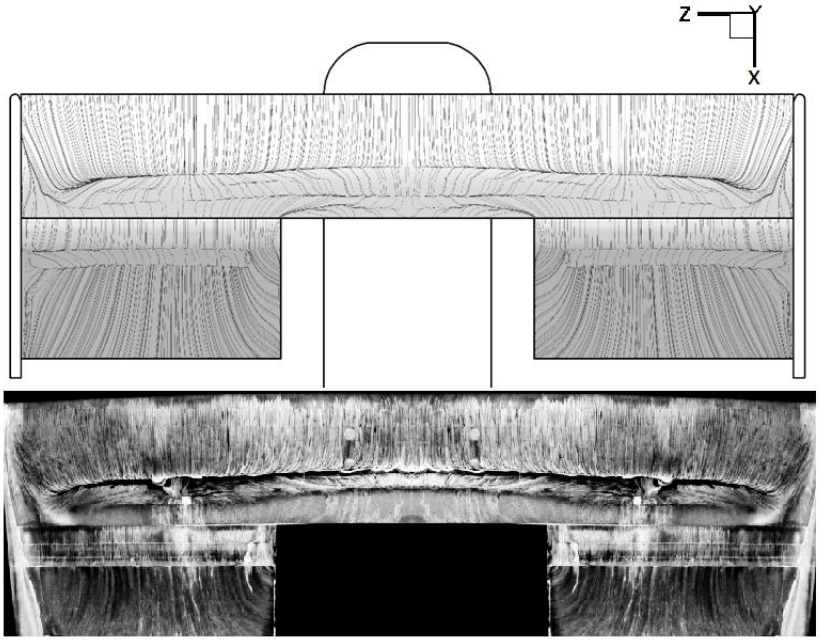

Figure 7. Surface flow on the suction surface of the main-plane and flap elements shown by CFD streaklines (top) and wind tunnel flow visualisation (bottom) (*h/c* = 0.177 and Re = 4.75 x 10^5)

5.2 Surface Pressures

Figure 8 shows the surface pressures generated by the wing in the straight-line condition and at 5° yaw. For the zero-yaw case the surface pressures appear symmetrical, as would be expected, whilst at yaw both the stagnation and low pressure locations are changed. This is shown quite dramatically on the nose tip as the stagnation point is shifted to the side. There appear to be larger areas of high pressure on the leeward upper main-plane surface as air stagnates on the inside of the endplate. Similarly, less suction is generated on the windward lower main-plane surface as the endplate blocks flow from entering the region below the wing, hence higher pressures can be observed on the windward endplate in Figure 8b. This increase of pressure on the leeward pressure surface and reduction of suction on the windward suction surface results in the leeward half of the wing producing more downforce than the other half. These effects were also noted by Gogel & Sakurai [21] for a wing operating out of ground effect. This effect would be amplified on-track, where aero-elasticity causes the leeward half to be pushed

closer to the road and increase downforce due to ground effect. As downforce has been shown to reduce when operating at yaw then clearly the leeward increase does not make up for the windward decrease.

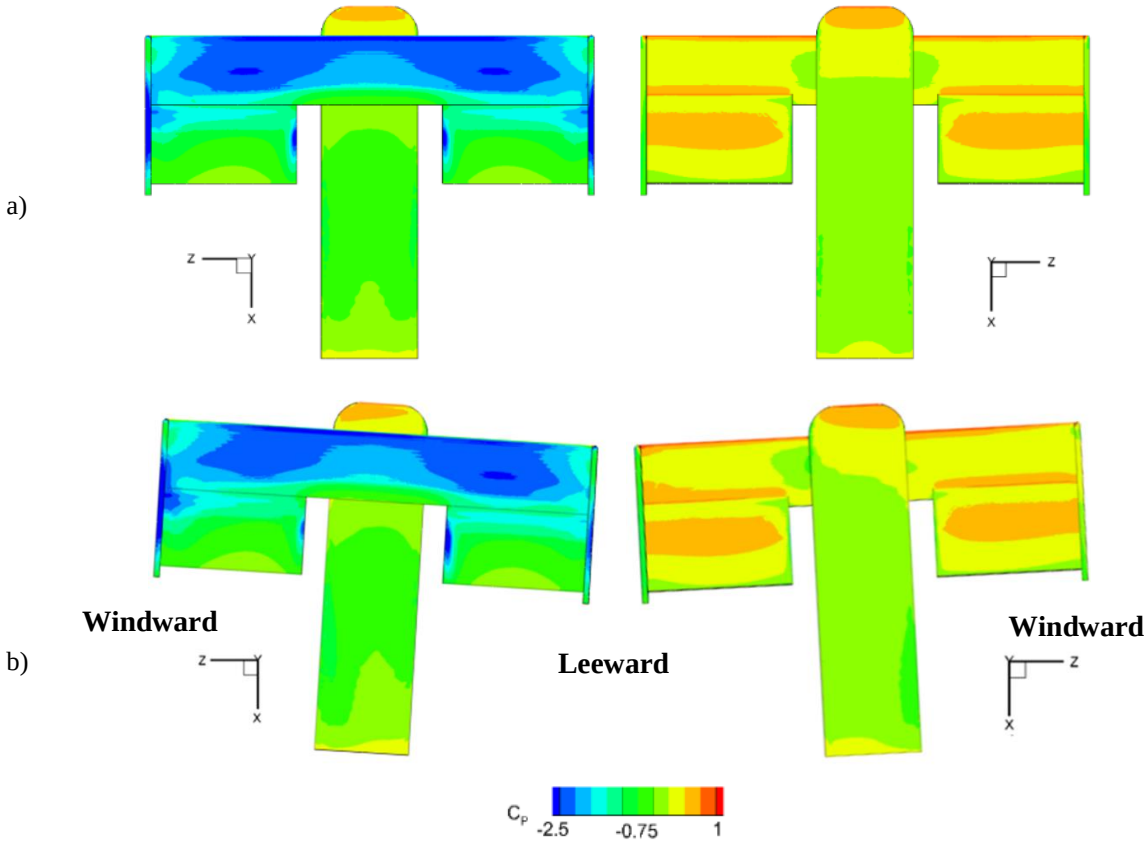

Figure 8. Contours of pressure coefficient on the upper (right-hand column) and lower surfaces (left-hand column) of the wing and nose assembly at *h/c* = 0.177 and Re = 4.75 x 10^5 for a) straight-ahead case and b) 5° yaw (flow moves in +ve x-direction)

The low pressure regions on the endplate and flap wing tip indicate the formation of vortices due to the circulation of flow from the higher to lower pressure regions. Based on the change of surface pressure in these regions it is clear that the strength of these vortices is altered when operating at yaw; this will be examined in detail in the next section.

Figure 9a shows the pressure distribution for the main plane at the wing centreline at both 0° and 5° of yaw. The pressure distribution again shows how maximum suction is generated close to the leading edge of the wing and that the laminar separation bubble occurs around $0.6 \leq x/c \leq 0.8$. The upper surface remains relatively unchanged other than a very slight increase in pressure at $x/c = 0.85$; which is likely due to air stagnating on the side of the pylon. The main difference is the lower surface of the wing, for which suction has been slightly reduced across its entire length, showing that the flow velocity and thus mass-flow rate must have been reduced. As previously postulated.

A comparison of the main-plane and flap pressure distribution, taken at the centreline of the flap, is shown in Figure 9b. It shows that at yaw only the leeward portion of the wing is affected, in comparison to the straight-ahead case, and that suction is lost in the range of 3–5.5% across the entire length of the main-plane element suction surface. Although it may not be clear in the graph, but there is also a reduction of the flap suction peak ($1 \leq x/c \leq 1.25$) of 2.1%. The pressure distribution on the windward side, however, lies almost perfectly over the zero-yaw distribution. It should be remembered, however, that these graphs only show two spanwise locations, nevertheless their results are still valid and important.

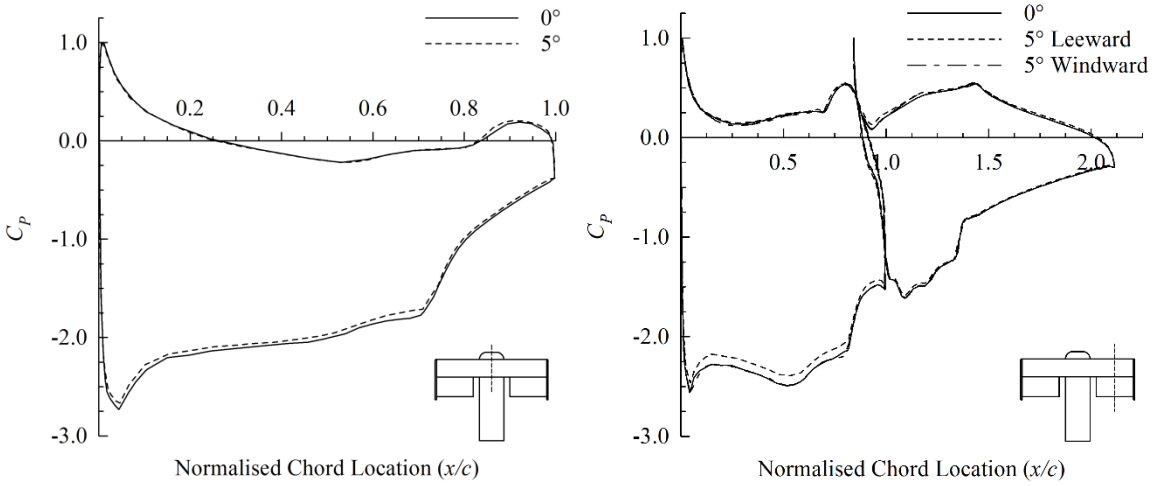

a) b)

Figure 9. Pressure distribution of a) main-plane element at the wing centreline, and b) main-plane and flap at outboard location (shown on wing plan sketch)

5.3 Mass-flow Rate

It was postulated previously that a change in mass-flow rate could have been the energy extraction mechanism which caused trailing-edge separation only in the yawed case. Hence the mass-flow rate through a plane bounded by the wing suction surface, endplate inner edge and ground plane (Figure 10) was evaluated. It was found that the mass-flow rate decreased from 1.706 kg/s for the straight-ahead wing to 1.684 kg/s for the wing orientated at 5° yaw. This 0.022 kg/s reduction in mass-flow rate is equivalent to a 0.532 ms^{-1} reduction in average velocity under the wing and in turn a 1.663% reduction in kinetic energy of the flow at the test ground clearance of h/c = 0.177.

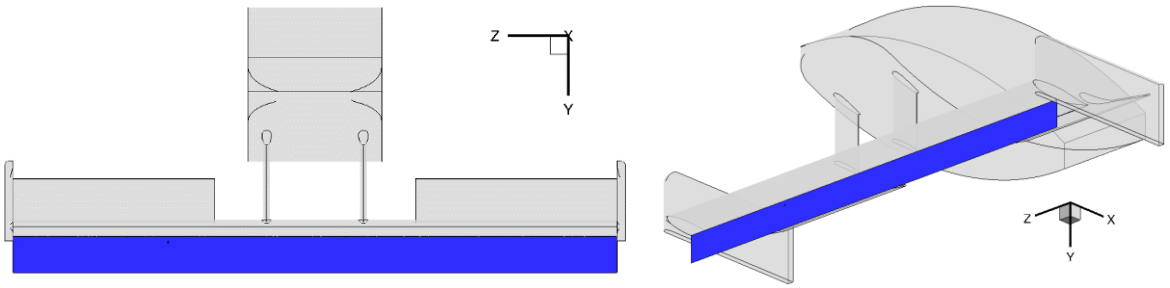

Figure 10: Plane between suction surface and ground where mass-flow rate was calculated

5.4 Wake structures

Vortices produced near to the endplate of a single-element and double-element wing in ground effect were observed by Zhang et al. [7] and Zhang & Zerihan [9] through surface flow visualisation and PIV (Particle Image Velocimetry) velocity measurements. The formation of vortices on the lower inside edge and upper outside edge of the endplate, as shown in Figure 11a, show similarity to those observed in these previous studies. The lower vortex is formed as the higher pressure freestream flow moves laterally towards the main-plane suction surface whilst the upper vortex is due to the air moving away from the higher pressure on the flap's upper surface, over the endplate, to the lower freestream pressure. Zhang & Zerihan used a wing with a single flap, which covered the entire wing span, unlike the two individual flaps used in the present study, hence two additional vortices are formed at the inner flap tips in the current case.

The development of vortices downstream is shown in Figure 11 for both the 0° and 5° yaw orientations. Iso-surfaces of the Q criterion for Q = 2000 s^{-2} are plotted in Figure 11d. Q-criterion defines a vortex as occuring when Q, the second invariant of the velocity gradient tensor, is positive and the pressure is lower than ambient. Essentially, it represents the local balance between vorticity magnitude (Ω) and strain rate (S) and defines vortices as areas where the vorticity magnitude is larger than the magnitude of rate-of-strain (Equation 1).

$$Q = 0.5\,(\Omega^2 + S^2) \qquad (1)$$

There is noticeable dissipation and lateral inward movement of all vortices originating from the wing. The flap vortices are smaller in size than the main-plane wing-tip vortex, a consequence of the smaller amount of downforce the flap produces. Whilst there is an inboard movement of the cores, this could be a result of the nose section which creates a lower pressure underneath itself towards which the flap vortex moves. Lower-than-freestream pressure regions on both the upper and lower surfaces of the body are apparent by observation of the vortices forming from it; these vortices begin at the stagnation region on the nose and then develop along each

edge of the body. Whilst the rearward half of this body is not representative of an actual car, the frontal half certainly is and thus shows that the nose of a monoposto racing car will generate vortex structures.

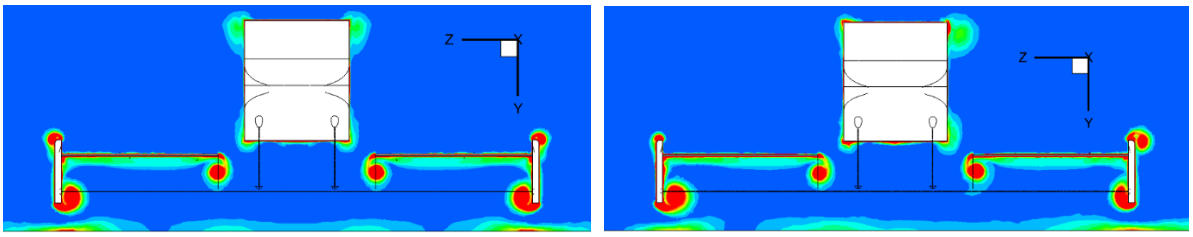

a) 0c behind trailing edge of flap, 0° yaw (left) and 5° yaw (right)

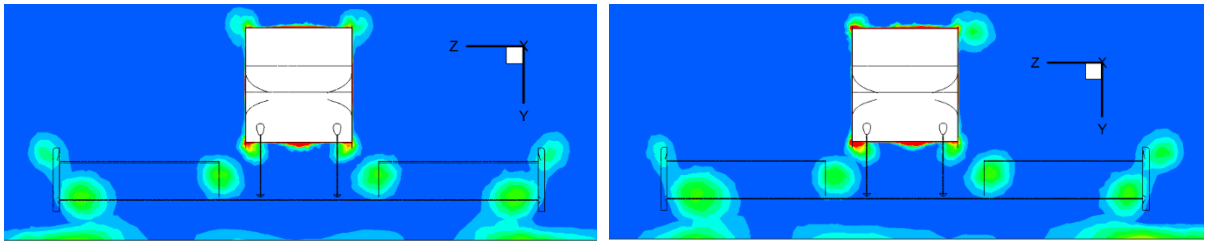

b) 0.6c behind trailing edge of flap, 0° yaw (left) and 5° yaw (right)

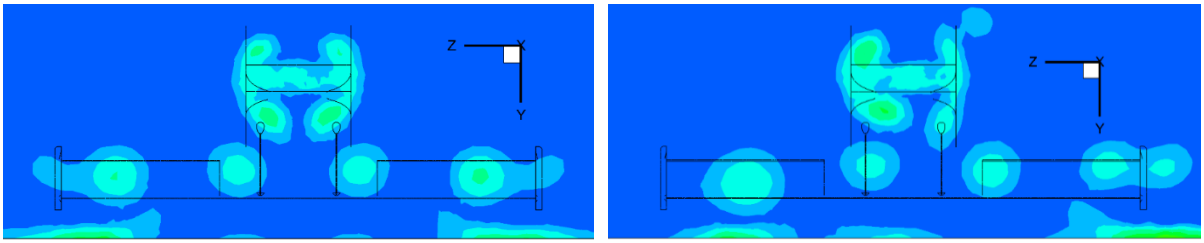

c) 1.4c behind trailing edge of flap, 0° yaw (left) and 5° yaw (right)

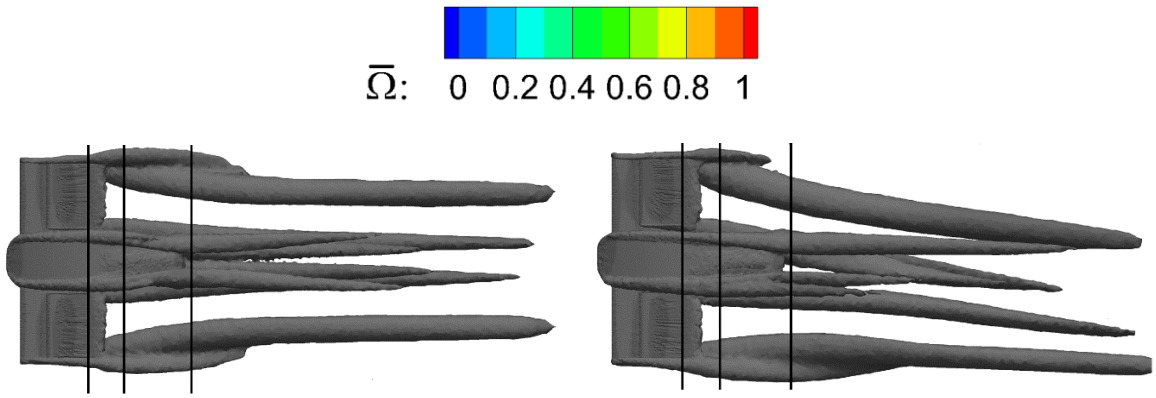

d) Iso-surface of Q criterion with lines indicating the locations of planes a-c

Figure 11. CFD results for 0° (left) and 5° (right - lateral flow component in –z direction) yaw at *h/c* = 0.177 and Re = 4.75 x 10^5. (a-c) Contours of normalised vorticity magnitude ($\bar{\Omega}$) and (d) iso-surfaces of Q = 2000 s^{-2}

The wing-tip vortex which forms on the lower-inner edge of the endplate is the strongest of all the vortices which are formed. As described earlier, this vortex has a force-enhancing capability through both the low pressure it produces on the lower surface of the wing, but also the constraining of flow due to its inboard movement. At 5° yaw the windward vortex is strengthened, as postulated in previous sections, due to the larger pressure gradient occurring across the endplate. This is a result of air stagnating on the side of the endplate in the yawed case rather than on the frontal surface. The now-larger vortex then moves inboard towards the central region as it travels parallel with the freestream flow.

The upper endplate vortex is noticeable, but much weaker than the other two vortices (as shown by its lower vorticity in Figure 7b & 7c). This is completely a function of the much smaller pressure gradient between the upper region endplate and freestream air, approximately $\Delta C_P=0.3$ as opposed to $\Delta C_P=1.45$ between the freestream and main-plane suction surface. Whilst both the main-plane and flap vortices move upwards as they travel downstream, a result of the upwash due to downforce, the endplate vortex moves downwards as it moves towards the low pressure core of the wing-tip vortex. At yaw, the stagnation of air on the outside of the windward endplate completely inhibits the formation of the upper-endplate vortex, hence it is not visible in Figure 11c. By contrast, the leeward upper endplate vortex is strengthened to a level comparable to the main-plane wing-tip vortex. The flap vortices are least affected by the change in wind direction, this is most likely due to the pressure gradient across them changing only slightly and there being no large surface for the air to stagnate on, unlike the vortices which form at the endplates. At the leeward endplate, stagnation on the inside of the endplate reduces the pressure gradient forming the main-plane tip vortex, thus weakening it, but increases it on the upper surface hence producing a much stronger vortex on the upper endplate. Whilst in straight-ahead flow the wing-tip vortex dominates this region, at yaw two vortices occur that are almost identical in strength. Stagnation on the outside of the windward endplate has the completely opposite effect, strengthening the main-plane tip vortex but inhibiting the upper-endplate vortex (Figure 11c). As indicated previously by the surface pressures, the magnitude and trajectory of all vortices has been altered significantly due to a change in local flow direction and surface pressure gradient. Vortices move in parallel with the freestream flow direction, hence their trajectory relative to the model has been altered. At yaw, all vortices generated by a lateral movement of air in the same direction as the freestream air (i.e. in the –z direction) increase in strength, whereas those which form due to air moving in the opposite direction are weakened. This is solely due to the wind either helping or inhibiting the lateral movement of air.

6. Conclusions

Whilst previous studies of wings in ground effect have focused on pitch and ground clearance sensitivity, there is a lack of studies into yaw effects on a geometry representative of current-era racing car front wings. The yawed condition occurs when a race car is cornering, which is the area where downforce is primarily required. As such it is common practice for racing teams to look at the stability and sensitivity of the car in yaw as well as in pitch and heave. The aim of the present study was thus to investigate the quasi-static testing approach regularly taken by race car aerodynamicists, but never published for competitive reasons, to simulate the car operating in yawed conditions such as during cornering or in a crosswind.

Wind tunnel testing and computational simulation of the model at degrees of yaw representative of those experienced by a racing car on-track showed that aerodynamic performance in terms of downforce generation was lost as the yaw angle was increased. The largest loss was seen at the lowest ground clearances, in the force-reduction regime, however, even at higher clearances in which a wing would typically operate the downforce loss was more than 20 points (~1.5% $-C_L$ loss). So although this may not appear large, it is significant in racing terms where the difference between cars comes down to tenths of a second. The reduction in forces is attributed to a change in stagnation locations and a reduction in the effective diffuser angle of the wing's suction surface causing a reduction of mass flow under the wing. Although the change in forces and surface flow structures were not drastic, it should be remembered that the flow structures produced by the wing are also very important and these were shown to be altered significantly. Due to the yawed condition, vortices which formed due to the lateral movement of air in the same direction as the air's relative lateral velocity component were strengthened, whilst those which formed in the opposite direction were inhibited. This resulted in a highly asymmetrical wake which was amplified in the far-wake region as vortices moved parallel to the wind direction. This may have implications for wheel-wake management and other downstream features which operate in the wake of the front wing. Additionally, for a full car, unlike an isolated front wing, the results between a yawed case and a curved-flow simulation will be much larger due to the greater difference in flow angles.

The 3-equation $k\text{-}k_L\text{-}\omega$ turbulence model was employed due to a large separation bubble occurring on the wing. Although the model was capable of predicting the separation bubble shape and location, in terms of separation and reattachment positions, it did not appear to model correctly the magnitude of turbulent kinetic energy produced in the separation-induced transition phenomena. Hence the still-laminar boundary layer separated a second time. Despite struggling to represent turbulent reattachment the model showed good correlation

with wind tunnel results in terms of forces and general surface flow structures, and thus allowed the off-surface flow features to be analysed.1

This study has shown the fundamental flow physics of a wing operating at yaw, which race car aerodynamicists are working to control. In Formula One complex endplates with holes, slots, vortex generators and turning vanes have been used to improve the stability and sensitivity of the car in yaw to produce a consistent downforce platform when cornering. The use of simple 'two-dimensional' endplates in this study has shown why these features are common: to alleviate stagnation on the windward surface and separated areas on the leeward surface, and to control the direction of wake structures.

A racing car must maximise its downforce production during cornering, when it will inevitably be operating at some yaw angle, rather than on straights so it is important to understand the fundamental flow physics of such conditions. This study has used a simplified model to show these fundamental aspects so that the decisions made by top-level motorsport teams, which are rarely published, can be understood and applied elsewhere. Using this as a starting point the effect of additional complexities to the design and their individual effects on the flow field could be observed.

References

[1] Knowles K, Donogue D T and Finnis M V. A Study of Wings in Ground Effect. In: RAeS Vehicle Aerodynamics Conference, Loughborough, UK, 1994.

[2] Ranzenbach R and Barlow J B. Two-Dimensional Airfoil in Ground Effect, An Experimental and Computational Study. SAE Paper 94-2509, 1994.

[3] Ranzenbach R and Barlow J B. Cambered Airfoil in Ground Effect - Wind Tunnel and Road Conditions. AIAA paper no. 95-1909, 1995.

[4 Ranzenbach R and Barlow J B. Cambered Airfoil in Ground Effect: An Experimental and Computational Study. SAE Paper 96-0909, 1996.

[5] Ranzenbach R and Barlow J B. Multi-element Airfoil in Ground Effect- an Experimental and Computational Study. AIAA paper no. 97-2238, 1997.

[6] Zerihan J and Zhang X. Aerodynamics of a Single-Element Wing in Ground Effect. Journal of Aircraft 2000; 37(6): 1058-1064.

[7] Zhang X, Zerihan J, Ruhrmann A and Deviese M. Tip Vortices Generated by a Wing in Ground Effect. In: 11th International Symposium on Applications of Laser Techniques to Fluid Mechanics, Instituto Superior Tecnico, Lisbon, Portugal, 2002.

[8] Zhang X and Zerihan J. Aerodynamics of a Double Element Wing in Ground Effect. AIAA Journal 2003; 45(6): 1007-1016.

[9] Zhang X and Zerihan J. Edge Vortices of a Double-Element Wing in Ground Effect. Journal of Aircraft 2003; 41(5): 1127-1137.

[10] Correia J, Roberts L S, Finnis M V and Knowles K. Scale Effects on a Single-Element Inverted Wing in Ground Effect. The Aeronautical Journal 2014; 118: 797-809.

[11] Dominy R G. Aerodynamics of Grand Prix Cars. Proceedings of the Institute of Mechanical Engineers, Part D: Journal of Automobile Engineering 1992; 206(4): 267-274.

[12] Zhang X, Toet W and Zerihan J. Ground Effect Aerodynamics of Racing Cars. Applied Mechanics Review 2006; 59(1): 33-49.

[13] Molina J and Zhang X. Aerodynamics of a Heaving Airfoil in Ground Effect. AIAA Journal 2011; 49(6): 1168-1179.

[14] Toet W. Aerodynamics and Aerodynamic Research in Formula 1. The Aeronautical Journal 2013; 117 1-26.

[15] Agathangelou B and Gascoyne M. Aerodynamic Design Considerations of a Formula 1 Racing Car. In: SAE International Congress & Exposition, Detroit, MI, 1998, 980399.

[16] Dominy R G. The Influence of Slipstreaming on the Performance of a Grand Prix Racing Car. Proceedings of the Institute of Mechanical Engineers, Part D: Journal of Automobile Engineering 1990; 204(1): 35-40.

[17]Soso M D and Wilson P A. Aerodynamics of a Wing in Ground Effect in Generic Racing Car Wake Flows. Proceedings of the Institute of Mechanical Engineers, Part D: Journal of Automobile Engineering 2006; 220(1): 1-13.

[18] Soso M D and Wilson P A. The Influence of an Upstream Diffuser on a Downstream Wing in Ground Effect. Proceedings of the Institute of Mechanical Engineers, Part D: Journal of Automobile Engineering 2008; 222(4): 551-563.

[19] Correia J, Roberts L S, Finnis M V and Knowles K. Aerodynamic Characteristics of a Monoposto Racing Car Front Wing Operating in High Turbulence Conditions. International Vehicle Aerodynamics Conference 2014, Loughborough, UK. Paper C1385 015.

[20] Newbon J, Dominy R G and Sims-Williams D B. Investigation into the Effect of the Wake from a Generic Formula One Car on a Downstream Vehicle. International Vehicle Aerodynamics Conference 2014, Loughborough, UK. Paper C1385 005

[21] Gogel D and Sakurai H. The Effects of End Plates on Downforce in Yaw. SAE Paper 2006-01-3647, 2006.

[22] Knowles K and Finnis M V. Development of a New Open-jet Wind Tunnel and Rolling Road Facility. In: 2nd MIRA Int. Conf. on Vehicle Aerodynamics, Coventry, 1998.

[23] ANSYS Fluent, Release 15.0.07, 2014, 2600 ANSYS Drive, Canonsburg, PA 15317, USA. www.ansys.com

[24] ANSYS ICEM CFD, Release 15.0, 2014, 2600 ANSYS Drive, Canonsburg, PA 15317, USA. www.ansys.com

[25] Walters D K and Cokljat D. A Three-Equation Eddy-Viscosity Model for Reynolds-Averaged Navier–Stokes Simulations of Transitional flow. Journal of Fluids Engineering 2008; 130(12).

[26] Lanfrit M. Best Practice Guidelines for Handling Automotive External Aerodynamics with FLUENT, Version 1.2, Guide, Darmstadt: Fluent Deutschland GmbH. 2005.

[27] Dominy J A and Dominy R G. Aerodynamic Influences on the Performance of the Grand Prix Racing Car. Proceedings of the Institute of Mechanical Engineers, Part D: Journal of Automobile Engineering 1984; 198(2): 87-93.

[28] Turner C. Laminar Kinetic Energy Modelling for Improved Laminar-Turbulent Transition Prediction. PhD Thesis: The University of Manchester, Faculty of Engineering and Physical Sciences. 2012.